DTU Library

Modeling the use of sulfate additives for potassium chloride destruction in biomass combustion

Wu, Hao; Grell, Morten Nedergaard; Jespersen, Jacob Boll; Aho, Martti; Jappe Frandsen, Flemming; Glarborg, Peter

Link back to DTU Orbit

MODELING THE USE OF SULFATE ADDITIVES FOR POTASSIUM CHLORIDE DESTRUCTION IN BIOMASS COMBUSTION

Hao Wu*,[1], Morten Nedergaard[1], Jacob Boll Jespersen[1], Martti Aho[2], Flemming Jappe Frandsen[1], Peter Glarborg[1]
[1] Department of Chemical and Biochemical Engineering, Technical University of Denmark, Søltofts Plads, Building 229, DK-2800 Kgs. Lyngby, Denmark
[2] VTT Technical Research Centre of Finland, P.O. Box 1603, FI-40101, Jyväskylä, Finland
* Corresponding Author. Phone:+45 4525 2927, Fax:+ 45 4588 2258, Email:haw@kt.dtu.dk

ABSTRACT: Potassium chloride, KCl, formed from biomass combustion may lead to ash deposition and corrosion problems in boilers. Sulfates are effective additives for converting KCl to the less harmful K_2SO_4. In the present study, the decomposition of ammonium sulfate, aluminum sulfate and ferric sulfate was studied respectively in a fast-heating rate thermogravimetric analyzer (TGA) for deriving a kinetic model. The yields of SO_2 and SO_3 from the decomposition were studied in a tube reactor, revealing that the ratio of the SO_3/SO_2 released varied for different sulfate and for ammonium sulfate the ratio was affected by the decomposition temperature. Based on the experimental data, a model was proposed to simulate the sulfation of KCl by different sulfate addition, and the simulation results were compared with pilot-scale experiments conducted in a bubbling fluidized bed reactor. The simulation results of ammonium sulfate addition and ferric sulfation addition compared favorably with the experimental results. However, the model for aluminum sulfate addition under-predicted significantly the high sulfation degree of KCl observed in the experiments, possibly because of an under-estimation of the decomposition rate of aluminum. Under the boiler conditions of the present work, the simulation results suggested that the desirable temperature for the ferric sulfate injection was around 950-900°C, whereas for ammonium sulfate the preferable injection temperature was below 800°C.
Keywords: additives, alkali, biomass, combustion, modeling, ashes

1 INTRODUCTION

One of the major technical challenges associated with the use of biomass through combustion technologies is that biomass combustion may result in a considerable amount of alkali chlorides in the flue gas and subsequently lead to severe deposition and corrosion problems in the boiler [1-6]. In order to mitigate the alkali chloride-induced problems, a feasible method is to use additives to convert the alkali chlorides to the less harmful species [7]. Sulfates, including ammonium sulfate, aluminum sulfate and ferric sulfate, have been proven to be very effective in converting the alkali chlorides to the less harmful alkali sulfates [8-10]. The high effectiveness of the sulfate additives are mainly related to the SO_3 released during their thermal decomposition, which reacts with alkali chlorides efficiently [11,12]. However, despite the presence of extensive experimental investigations on the use of sulfate additives under different boiler conditions [8-10], fundamental studies on the decomposition rate and products of sulfate additives are scare. In relation to this, no modeling work has been carried out to describe the sulfation of alkali chlorides by sulfate addition during biomass combustion. The lack of such knowledge generally limits the optimal use of the sulfate additives.

The objectives of this study were to understand the decomposition behavior of ammonium sulfate, aluminum sulfate and ferric sulfate under boiler conditions, and to develop a model to describe the sulfation of KCl by sulfate addition during biomass combustion. The decomposition of the sulfates was studied respectively in a fast-heating rate thermogravimetric analyzer (TGA) and a tube reactor. The model developed in this work involved a description of sulfate decomposition, a detailed gas-phase kinetic model for sulfation of potassium chloride based on [12], and a simplified model for homogeneous and heterogeneous nucleation of potassium sulfate [13]. The simulation results of sulfate addition were compared with the experimental results from biomass combustion on a pilot-scale bubbling fluidized bed reactor where ammonium sulfate, aluminum sulfate and ferric sulfate was injected respectively to the freeboard of the reactor. Besides, the effectiveness of different sulfate was compared through simulation.

2 EXPERIMENTAL

2.1 Fast heating rate TGA

Thermal decomposition of ammonium sulfate, aluminum sulfate and ferric sulfate was studied respectively in a fast heating rate Netzsch STA 449 F1 Jupiter thermogravimetric analyzer (TGA). The experiments were carried out under N_2 atmosphere, using pure and dehydrated sulfates. During the experiments, the sulfate was heated at a rate of 500°C/min to an end temperature, and then kept isothermally. The mass loss during the isothermal period was recorded and used to derive the kinetic parameters of sulfate thermal decomposition. For the different sulfate, the end temperatures applied in the experiments differed. For the experiments of ammonium sulfate, the end temperatures were chosen to be in a range of 200–350°C. For the ferric sulfate experiments, the end temperatures varied from 600°C to 800°C. For the aluminum sulfate experiments, the range of the end temperatures was 700–800°C.

2.2 Laboratory-scale tube reactor

In order to study the yields of SO_2 and SO_3 from the thermal decomposition of ammonium sulfate, aluminum sulfate and ferric sulfate, experiments were conducted in a laboratory-scale tube reactor. The principles of the reactor and the experiments have been described in detail in our early work [14,15]. In the reactor, the decomposition of sulfate was carried out under well-defined temperature and flow conditions (5 Nl/min N_2), and the SO_2 released were analyzed continuously by an IR-based gas analyzer. Based on the analyzed SO_2

concentrations over time, a fractional conversion of the sulfur in ferric sulfate to SO_2 at the given temperature condition was calculated. The remaining sulfur in ferric sulfate is assumed to be released as SO_3. The temperature range studied was 500–1000°C, where the conversion of SO_3 to SO_2 is expected to be negligible.

2.3 Bubbling fluidized bed pilot reactor

Pilot-scale experiments were conducted in the 20 kW bubbling fluidized bed (BFB) reactor at the VTT Technical Research Centre of Finland. The fuel used in the experiments was a mixture of 60% (energy basis) bark and 40% (energy basis) refuse derived fuel (RDF) comprised mainly of packaging waste from households and industry. The properties of the fuel mixture are given in Table I. The additives used in the experiments were ammonium sulfate, aluminum sulfate, and ferric sulfate aqueous solutions.

Table I: Properties of the fuel mixture of 60% (energy basis) bark and 40% RDF.

Properties	Unit	Fuel mixture
Moisture	(wt%, ar)	30.0
Volatiles	(wt%, db)	76,6
Ash 815°C	(wt%, db)	5.0
Ash 550°C	(wt%, db)	5.6
C	(wt%, db)	52.0
H	(wt%, db)	6.7
N	(wt%, db)	0.43
S	(wt%, db)	0.08
Cl	(wt%, db)	0.237
K	(wt%, db)	0.20
Na	(wt%, db)	0.19
Ca	(wt%, db)	1.21
LHV	(MJ/kg, db)	22.9
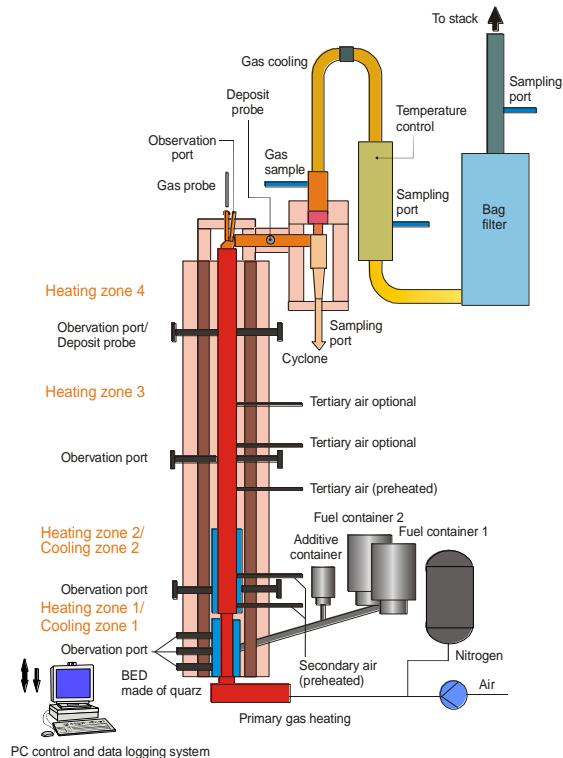
Figure 1: Schematic diagram of the bubbling fluidized bed reactor [9].

A schematic diagram of the BFB reactor is shown in Figure 1. During the experiments, the fuel was fed into the bed with screw-type feeder. The ratio between the primary (fluidizing), second and tertiary air was 50:30:20. The fuel feeding rate was kept at 2.48 kg/h (dry basis), and the total air feeding rate was 278 Nl/min. The measured (by thermocouples) temperature distribution as a function of the residence time in the reactor is shown in Figure 2. It can be seen that the freeboard temperature varied, with the highest temperatures measured close to the secondary and tertiary air inlets.
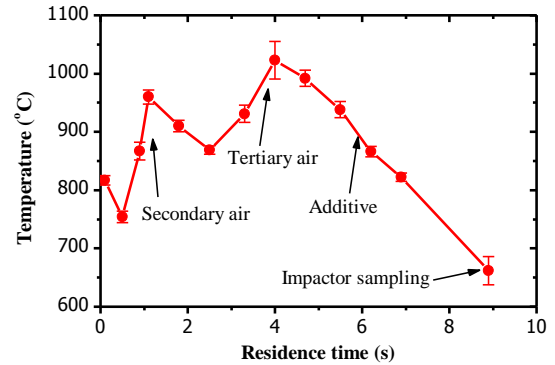
Figure 2: Temperature distribution versus gas residence time in the BFB reactor.

The sulfate additive was sprayed co-currently to the upper part of the freeboard through a nozzle. The residence time corresponding to the additive injection position was 5.8 s, as illustrated in Figure 2. The mean droplet size of the spray was about 10 μm. The amount of the additive injected was determined based on the fuel Cl content and feeding rate. The molar ratio of $S_{additive}/Cl_{fuel}$ was chosen to be 0.225 and 0.75 respectively for the different sulfate.

The aerosols generated in the reactor were collected by a low pressure impactor at flue gas temperatures of about 650°C. The compositions of the aerosols (<4 μm) were analyzed by ion chromatography (IC) for the Cl and S content and by flame atomic absorption spectroscopy (FAAS) for the alkali content.

3 MODEL DEVELOPMENT AND SIMULATION

3.1 Deposition of sulfate

The decomposition of sulfate is assumed to be kinetically controlled and follow the volumetric reaction model:

$$\frac{dW}{dt} = -kW \qquad (1)$$

where W is the relative mass of the anhydrous ferric sulfate defined as:

$$W = \frac{m - m_\infty}{m_0 - m_\infty} \qquad (2)$$

where m_0 (g) is the mass of the anhydrous sulfate before decomposition, m_∞ (g) is the mass of the residue after complete decomposition, and m(g) is the mass of anhydrous sulfate at t (s) during decomposition.

The rate constant k in Eq. 1 follows an Arrhenius expression:

$$k = A \cdot \exp(-\frac{E}{RT}) \qquad (3)$$

where A (s^{-1}) is the pre-exponential factor, E (kJ/mol) the activation energy, R (kJ/mol/K) the gas constant, and T (K) the temperature of the particle.
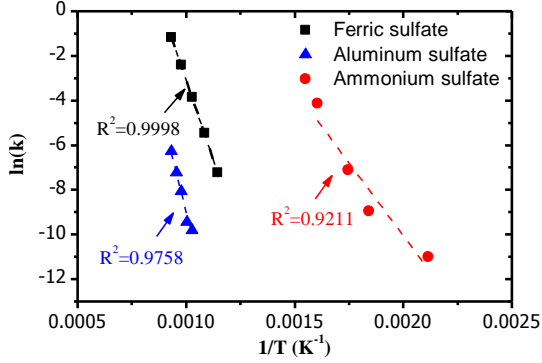

Figure 3: Correlation between ln(k) and 1/T during the decomposition of different sulfate in the TGA experiments under isothermal conditions.

The activation energy (E) and the pre-exponential factor (A) in Eq. 3 are derived from the TGA experiments. As shown in Figure 3, during the isothermal periods of the TGA experiments, a high linearity is generally seen between ln(k) and 1/T, indicating that Eq. 3 can satisfactorily describe the decomposition of the sulfates. Besides, it is also shown that the decomposition rate of sulfates studied in this work generally follows an order of ammonium sulfate>ferric sulfate>aluminum sulfate. The activation energy (E) and the pre-exponential factor (A) derived from Figure 3 for different sulfates are given in Table II.

**Table II:** Activation energy and pre-exponential factor derived from Figure 2.

|	E/R (K)	A (s^{-1})
Ammonium sulfate	13042	9.15E+06
Ferric sulfate	28480	1.08E+11
Aluminum sulfate	38782	8.70E+12
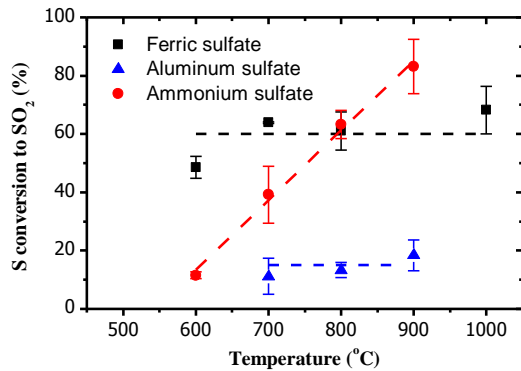
Figure 4: Yields of SO$_2$ (%) during decomposition of sulfate under different temperatures, the remaining sulfur is assumed to be released as SO$_3$. The dash lines show the yields of SO$_2$ used in the simulation.

Figure 4 shows the results from the laboratory-scale tube reactor experiments. For ferric sulfate, it can be seen that approximately 60% of the sulfur in ferric sulfate is released as SO$_2$ in the temperature range of 700–1000°C. Since the decomposition of ferric sulfate in a furnace primarily occurs at temperatures above 700°C, it is reasonable to assume for modeling purposes that 60% of

the sulfur from ferric sulfate decomposition is released as SO$_2$, whereas the remaining 40% is released as SO$_3$. This leads to the following equation for ferric sulfate decomposition:

$$Fe_2(SO_4)_3 \rightarrow Fe_2O_3 + 1.2SO_3 + 1.8SO_2 + 0.9O_2 \qquad (4)$$
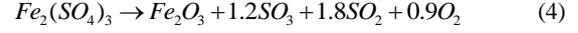
For aluminum sulfate, the yields of SO$_2$ are much smaller than that of ferric sulfate, and it is not significantly influenced by decomposition temperature. Therefore, in the modeling, we assume that 15% of the sulfur of aluminum sulfate is released as SO$_2$ and the remaining 85% is released as SO$_3$. This leads to the following equation for aluminum sulfate decomposition:

$$Al_2(SO_4)_3 \rightarrow Al_2O_3 + 2.55SO_3 + 0.45SO_2 + 0.225O_2 \quad (5)$$
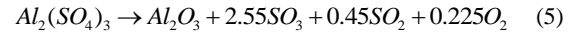
For the decomposition of ammonium sulfate, the yields of SO$_2$ increase almost linearly with increasing temperatures (see Figure 4). Therefore, in the modeling, a linear correlation shown as in the dash line in Figure 4 is adopted to simulate the yields of SO$_2$ from ammonium sulfate decomposition at different temperatures, and the remaining sulfur is assumed to be released as SO$_3$. The global decomposition reaction for ammonium sulfate can be written as:

$$(NH_4)_2SO_4 \rightarrow 2NH_3 + H_2O + (1-x)SO_3$$
$$+ xSO_2 + \frac{x}{2}O_2 \qquad (6)$$
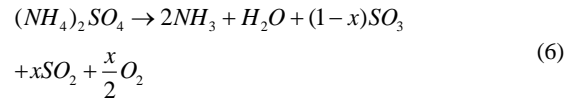
where x is the S conversion to SO$_2$ shown in Figure 4, which is dependent on the decomposition temperature of ammonium sulfate.

3.2 Detailed chemical kinetic model

Detailed chemical kinetic model is applied to describe the gas-phase reactions of the potassium, chlorine and sulfur species. The gas phase kinetic model used in this study was based on the reaction mechanism proposed by Hindiyarti et al [12], with updated the thermodynamic properties of the species KO$_2$.

3.3 Condensation of sulfate

For homogeneous and heterogeneous condensation of potassium sulfate, a first order reaction as used by Li et al. [13] is chosen to describe the processes:

$$K_2SO_4(g) \longrightarrow K_2SO_4(s) \qquad (7)$$

The rate constant for the reaction above, which represents the condensation rate predicted from aerosol theory [16], is:

$$k_{condensation} = 1 \times 10^{-61} \exp(150000/T) \qquad (8)$$

3.4 Simulation of the BFB reactor

In order to simulate the BFB experiments, the region from the sulfate injection location to the impactor sampling location (see Figure 2) was simulated as an ideal plug flow reactor. The simulation was carried out with CHEMKIN 4.1.1, using the plug-flow reactor model. The temperature profile used in the simulation was predefined based on the profile shown in Figure 2.

The amount and composition of the inlet flue gas were estimated based on the experiment without additive injection. The flue gas was assumed to contain only N$_2$, O$_2$, CO$_2$, H$_2$O, SO$_2$, HCl and KCl. The concentrations of N$_2$, O$_2$, CO$_2$ and H$_2$O were obtained by assuming that the fuel was fully converted in the reactor. The concentration of KCl was derived based on the amount of Cl in the

aerosols collected during the experiment without additive injection. Although the Cl collected in the aerosols contained both KCl and NaCl, in the simulation we assumed that the Cl found in the aerosols was only comprised of KCl. This assumption is believed to be reasonable since the molar ratio of K/Cl found in the aerosols was about 0.9, suggesting that KCl was dominated over NaCl. Besides, the sulfation rate of NaCl would be similar to that of KCl under boiler conditions. The HCl concentration in the flue gas was calculated by performing mass balance calculation on Cl, based on the amount of input fuel-Cl and the Cl collected as aerosols. Similarly, the SO_2 concentration was obtained from the mass balance calculation of S, according to the input fuel-S and the S collected as aerosols.

For the experiments with additive injection, a pseudo species, SO_3^*, which produces SO_2, SO_3 and O_2 upon decomposition (other gas/solid residues such as NH_3, Fe_2O_3 and Al_2O_3 were not considered in the simulation), was defined to simulate the additive in CHEMKIN. The kinetic parameters for suflate decomposition were based on Table II, and the product distribution was defined based on Eq. 4-6.

From the simulation results, the mass flow of Cl as aerosols was obtained by assuming that that all of the KCl and K_2Cl_2 found at the outlet of the reactor (i.e. the aerosol sampling location) were collected as aerosols.

3.5 Simulation for sulfate comparison

For comparing the effectiveness of the different sulfates and SO_3, simulation was carried out by using a temperature profile shown in Figure 5, which was estimated based on the cooling rate of the BFB reactor. The simulation was conducted with different sulfate additive and different additive injection temperature, as illustrated in Figure 5. The flue gas composition used in the simulation was the same as that used for simulating the BFB experiments, and the molar ratio of $S_{additive}/Cl_{fuel}$ was kept at 0.5.
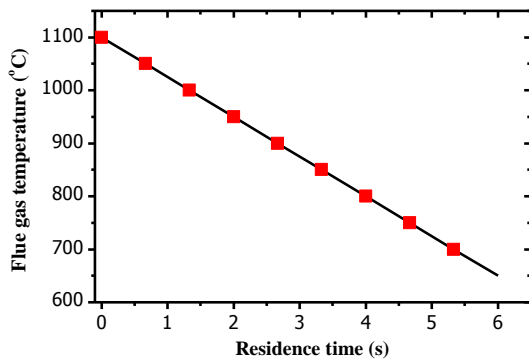

Figure 5: Temperature profile used for comparing the effectiveness of different sulfate and SO_3. The solid symbols denote the different additive injection temperature/position used in the simulation.

4 RESULTS AND DISCUSSION

4.1 Ammonium sulfate addition in the BFB reactor

Figure 6 compares the experimental and simulated mass flow of Cl (mg/Nm^3) in the aerosols during ammonium sulfate addition in the BFB reactor. It can be seen that the model generally captures the experimental

results well. The mass flow of Cl in the aerosols is slightly under-predicted by the model, implying a slight over-prediction of the effectiveness of ammonium sulfate addition on KCl sulfation. This is mostly like related to an over-estimation of the release of SO_3 from ammonium sulfate decomposition, which may be induced by the relative large experimental errors shown in Figure 4.
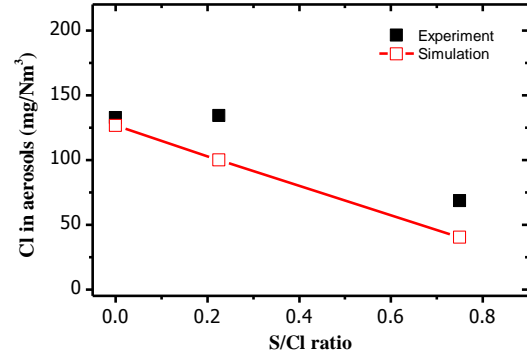
Figure 6: Comparison of the experimental and simulated mass flow of Cl (mg/Nm^3) in the aerosols during ammonium sulfate addtion under different molar ratios of $S_{additive}/Cl_{fuel}$.
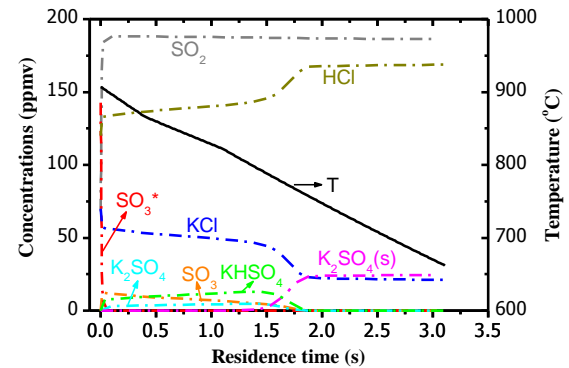
Figure 7: Concentration profiles of the major S and Cl species during the simulation of ammonium sulfate addition under a $S_{additive}/Cl_{fuel}$ ratio of 0.75.
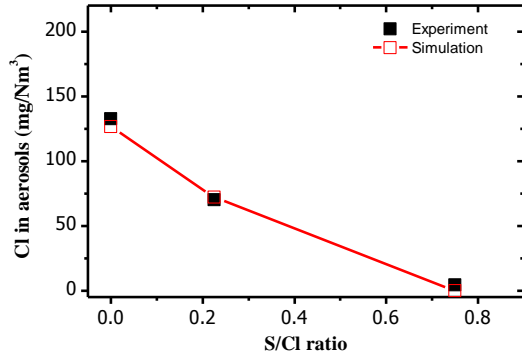
The distribution of the S and Cl species in the simulation zone during ammonium sulfate addition ($S_{additive}/Cl_{fuel}$ =0.75) is shown in Figure 7. It is seen that under the conditions of the BFB boiler, the decomposition of ammonium sulfate (denoted as SO_3^*) is completed almost instantaneously (~30 ms) after injection, forming both SO_2 and SO_3. The concentration of SO_2 becomes constant when the ammonium sulfate is completely decomposed, implying a negligible further conversion of SO_3 to SO_2. In the residence time of 0-1.5s, the sulfation of KCl appears to be thermodynamically constrained, reflected both by the small amount of K_2SO_4 formed, and the simultaneous presence of the reactive SO_3, $KHSO_4$ and KCl. In the residence time of about 1.5-2s, a rapid conversion of KCl is observed, which is accompanied by the formation of a considerable amount K_2SO_4 (s). This is mainly due to the occurrence of homogeneous and heterogeneous condensation of K_2SO_4 in the temperature range of 790-750 ℃, which removes the gaseous K_2SO_4 and promotes the following reactions of SO_3, $KHSO_4$ and KCl [11]:

$$KCl + SO_3(+M) = (KO_2)S(O)Cl(+M) \qquad (9)$$

$$(KO_2)S(O)Cl + H_2O = KHSO_4 + HCl \qquad (10)$$

$$KHSO_4 + KCl = K_2SO_4 + HCl \qquad (11)$$
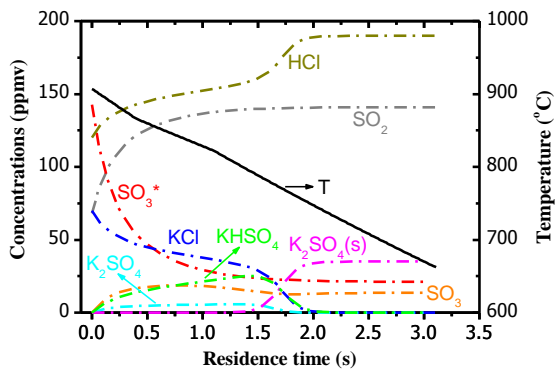
4.2 Ferric sulfate addition in the BFB reactor

A comparison of the experimental and simulated mass flow of Cl (mg/Nm^3) in the aerosols during ferric sulfate addition in the BFB reactor is shown in Figure 8. The simulation results are in good agreement with the experimental results. Both the experimental and simulation results indicate a rather complete sulfation of KCl under a $S_{additive}/Cl_{fuel}$ ratio of 0.75.

Figure 8: Comparison of the experimental and simulated mass flow of Cl (mg/Nm^3) in the aerosols during ferric sulfate addtion under different molar ratios of $S_{additive}/Cl_{fuel.}$

The distribution of the S and Cl species from the simulation of ferric sulfate is shown in Figure 9. It can be seen that the decomposition of ferric sulfate (denoted as SO$_3$*) is much slower than that of ammonium sulfate. Approximately 15% of the ferric sulfate remains unconverted at the outlet of the reactor. However, due to the high $S_{additive}/Cl_{fuel}$ molar ratio (0.75) and the significant release of SO$_3$ from ferric sulfate decomposition, the KCl in the flue gas is still fully converted to K$_2$SO$_4$. The conversion of KCl takes place primarily in the temperature range of 790-750°C, which is similar to that of ammonium sulfate addition.


Figure 9: Concentration profiles of the major S and Cl species during the simulation of ferric sulfate addition under a $S_{additive}/Cl_{fuel}$ ratio of 0.75.

4.3 Aluminum sulfate addition in the BFB reactor

Figure 10 presents a comparison of the experimental and simulated mass flow of Cl (mg/Nm^3) in the aerosols during aluminum sulfate addition in the BFB reactor. It appears that the model under-predicts significantly the effect of aluminum sulfate addition, resulting in a much higher mass flow of Cl in the aerosols than that obtained experimentally. According to the simulation results, only

less than 2% of the aluminum sulfate is decomposed under the conditions of the BFB reactor, which leads to a very low sulfation degree of the KCl in the flue gas. However, if the decomposition rate of aluminum sulfate is increased by 100 times, a reasonable good agreement is achieved between the experimental and simulation results (see the dotted line in Figure 10). Therefore, it is most likely that the decomposition rate of aluminum sulfate is under predicted. Compared to the BFB experiments where the aluminum sulfate is injected as liquid spray and is probably dried to nano-size particles before decomposition [9], the particle size of the aluminum sulfate used in the fast-heating rate TGA experiments is much larger. The difference in particle size may result in slower decomposition rate in the fast-heating rate TGA experiments. However, further investigations are needed in order to fully understand the decomposition behavior of aluminum sulfate under boiler conditions, which is outside the scope of this preliminary study.
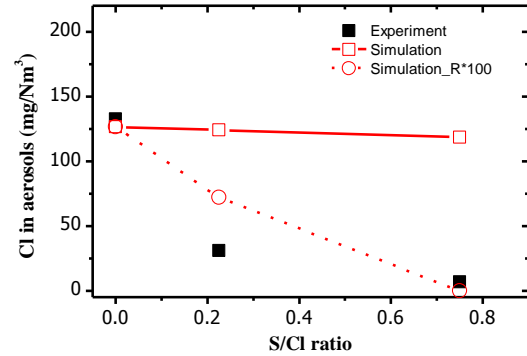
Figure 10: Comparison of the experimental and simulated mass flow of Cl (mg/Nm^3) in the aerosols during aluminum sulfate addtion under different molar ratios of $S_{additive}/Cl_{fuel}$. The dotted line shows the simulation results based on a decomposition rate 100 times higher than that estimated from the TGA experiments.

4.4 Comparison of the effectiveness of sulfate
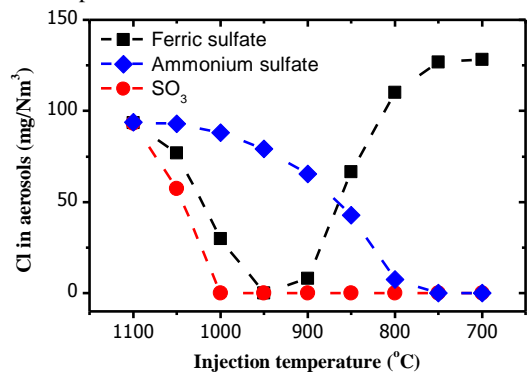
Figure 11: Comparison of the simulated effectiveness of ferric sulfate, ammonium sulfate and SO$_3$ under different injection temperatures according to the profile shown in Figure 5. The $S_{additive}/Cl_{fuel}$ molar ratio was kept at 0.5.

Figure 11 shows a comparison of the effectiveness of ferric sulfate, ammonium sulfate and SO$_3$ under different injection temperature conditions based on the temperature profile in Figure 5. The results of aluminum sulfate are not presented due to the significant difference between the simulation and experimental results.

It is seen from Figure 11 that the highest

effectiveness for ferric sulfate addition is achieved when it is injected at around 900-950°C, resulting in an almost complete destruction of the KCl in the flue gas. When the injection temperature is increased (e.g. 1100°C), the effectiveness of ferric sulfate is decreased due to a more pronounced dissociate of SO_3 to SO_2 at higher temperatures. However, when the injection temperature is decreased (e.g. 800°C), only a small fraction of ferric sulfate can be decomposed under the residence time conditions of Figure 5, which also limits the effectivness significantly.

The effectivness of ammonium sulfate appears to increase with decreasing injection temperature. This is mainly because that more SO_3 is released when the decompostiion of ammonium sulfate takes place at lower temperatures. Under a $S_{additive}/Cl_{fuel}$ molar ratio of 0.5, the KCl is almost totally sulfated when the ammonium sulfate is injected between 800-700°C. The high effectinvess of ammonium sulfate in this temprature range is mainly related to its fast decomposition rate and the significant release of SO_3 (see Figure 4).

The simulated effectiveness of pure SO_3 injection is also shown in Figure 11. It is seen that at high injection temperatures (e.g. 1100°C), the effectiveness of SO_3 is similar to that of ammonium sulfate and ferric sulfate, due to the rapid dissociation rate of SO_3. However, when injected below 1000°C, a complete sulfation of the KCl can be achieved under the simulation conditions. This is partly related to the large $S_{additive}/Cl_{fuel}$ molar ratio (0.5) used in the simulation, which greatly excess the stoichiometric ratio ($S_{additive}/Cl_{fuel}$=0.19) calculated based on the amount of KCl found in the flue gas.

5   CONCLUSION

The results of the present study showed that the yields of SO_3 from ferric sulfate and aluminum sulfate decomposition was almost independent of the decomposition temperature (up to 900°C), with ferric sulfate constantly producing about 40% SO_3 and aluminum sulfate generating about 85% SO_3. For ammonium sulfate, the yields of SO_3 decreased with increasing decomposition temperature. The models developed for KCl sulfation by ferric sulfate and ammonium sulfate addition captured the experimental results obtained in a bubbling fluidized bed (BFB) reactor well. However, the model for aluminum sulfate addition predicted a very low sulfation degree of KCl, which conflicted significantly with the high effectiveness of aluminum sulfate observed in the BFB experiments. This discrepancy is most likely related to an under-estimation of the decomposition rate of aluminum sulfate, which requires further investigations. Comparison of the effectiveness of ammonium sulfate and ferric sulfate through simulation suggested that under the boiler conditions similar to the present study, the desirable temperature for the injection of ferric sulfate was around 950-900°C, whereas for ammonium sulfate the preferable injection temperature was below 800°C.

7   REFERENCES

[1] Nielsen HP, Frandsen FJ, Dam-Johansen K, Baxter LL. The implications of chlorine-associated corrosion on the operation of biomass-fired boilers. Prog Energy Combust Sci 2000;26:283-98.

[2] Bashir MS, Jensen PA, Frandsen FJ, Wedel S, Dam-Johansen K, Wadenback J, Pedersen ST. Ash transformation and deposit build-up during biomass suspeinson and grate-firing: Full-scale experimental studies. Fuel Process Technol 2012;97:93-106.

[3] Frandsen FJ. Utilizing biomass and waste for power production—a decade of contributing to the understanding, interpretation and analysis of deposits and corrosion products. Fuel 2005;84:1277-94.

[4] Hupa M. Ash related issues in fluidized bed combustion of biomasses-recent research highlights. Energy Fuels 2012;26:4-14.

[5] Åmand LE, Leckner B, Eskilsson D, Tullin C. Ash deposition on heat transfer tubes during combustion of demolition wood. Energy Fuels 2006;20:1001-7.

[6] Aho M, Paakkinen K, Taipale R. Quality of deposits during grate combustion of corn stover and wood chip blends. Fuel 2013;104:476-87.

[7] Wu H, Glarborg P, Frandsen FJ, Dam-Johansen K, Jensen PA. Dust-firing of straw and additives: ash chemistry and deposition behavior. Energy Fuels 2011;25:2862-73.

[8] Aho M, Paakkinen K, Taipale R. Destruction of alkali chlorides using sulphur and ferric sulphate during grate combustion of corn stover and wood chip blends. Fuel 2013;103:562-9.

[9] Aho M, Vainikka P, Taipale R, Yrjas P. Effective new chemicals to prevent corrosion due to chlorine in power plant superheaters. Fuel 2008;87:647-54.

[10] Kassman H, Bäfver L, Åmand LE. The importance of SO_2 and SO_3 for sulphation of gaseous KCl-An experimental investigation in a biomass fired CFB boiler. Combust Flame 2010;157:1649-57.

[11] Glarborg P, Marshall P. Mechanism and modeling of the formation of gaseous alkali sulfates. Combust Flame 2005;141:22-39.

[12] Hindiyarti L, Frandsen F, Livbjerg H, Glarborg P, Marshall P. An exploratory study of alkali sulfate aerosol formation during biomass combustion. Fuel 2008;87:1591-600.

[13] Li B, Sun Z, Li Z, Aldén M, Jakobsen JG, Hansen S, Glarborg P. Post-flame gas-phase sulfation of potassium chloride. Combust Flame 2013;160:959-69.

[14] Wu H, Castro M, Jensen PA, Frandsen FJ, Glarborg P, Dam-Johansen K, Røkke M, Lundtorp K. Release and transformation of inorganic elements in combustion of a high-phosphorus fuel. Energy Fuels 2011:2886.

[15] Nielsen AR, Larsen MB, Glarborg P, Dam-Johansen K. High temperature release of SO2 from calcined cement raw materials. Energy Fuels 2011.

[16] Christensen KA, Livbjerg H. A plug flow model for chemical reactions and aerosol nucleation and growth in an alkali-containing flue gas. Aerosol Sci Tech 2000;33:470-89.